GLOBAL AND REGIONAL SEA LEVEL CHANGE

Manfred Wenzel and Jens Schröter

Alfred-Wegener-Institute for Polar and Marine Research, 27570 Bremerhaven, Germany

ABSTRACT

Sea level variations prior to the launch of satellite altimeters are estimated by analysing historic tide gauge records. Recently, a number of groups have reconstructed sea level by applying EOF techniques to gappy data. We complement this study with alternative methods. In a first step gaps in 178 records of sea level change are filled using the pattern recognition capabilities of artificial neural networks. Afterwards satellite altimetry is used to extrapolate local sea level change to global fields. Patterns of sea level change are compared to prior studies. Global mean sea level change since 1900 is found to be 1.65 ± 0.26 mm per year on average.

Key words: sea level; tide gauge; satellite altimeter; reconstruction; neural network.

1. INTRODUCTION

Global sea level rise is one of the major concerns in predicting climate and climate change for the decades to come. Projections for sea level rise have been compiled in the IPCC third and the 4th assessment report ([1] and [2] respectively). But still predictions vary substantially. It is important first to understand the magnitude of the past sea level change before we can reduce uncertainties in the future development. In this paper we will address the development of the global and the local sea level during the past century. Global sea level anomaly fields are reconstructed from tide gauges (TG's) for the period 1900-2009 in a two step procedure.

First we present an improved way to train a neural network to fill data gaps in time-series, e.g. from tide gauges. In [3] the network used for this purpose was trained using only time steps that have complete data. Here we describe a method that can deal with arbitrarily distributed missing values even during the training phase. Sea level anomaly are then calculated from these completed TG records. This is done by estimating their projection onto the principal components from the EOF decomposition of the altimetry data.

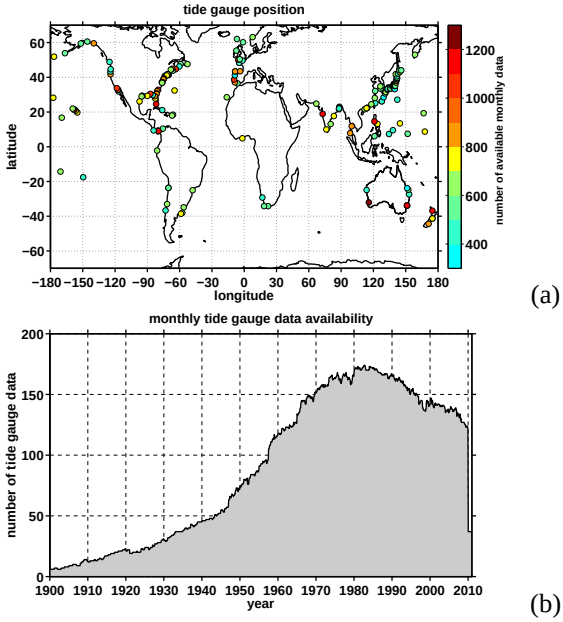

Figure 1. (a) Position of the selected tide gauges. The color coding gives the amount of available monthly data at the corresponding tide gauges. (b) Monthly data availability.

2. RECONSTRUCTION OF TIDE GAUGE DATA

For our purpose we selected the TG's in the latitudinal band 65^oS to 65^oN from the Permanent Service for Mean Sea Level (PSMSL) data archive [4] that have revised local reference (RLR) data and at least 30 annual mean values given. Thereof we excluded all data from the Mediterranean Sea, the North Sea, the Baltic Sea and the Sea of Japan. This selection finally gives 178 TG's whose spacial distribution is shown in Fig. 1 together with the availability of monthly data. It is obvious that many data are missing especially prior to 1950 and there is no month that has complete data. Thus the first task should be to fill these data gaps in an appropriate way. As in [3] all computations to reconstruct the missing TG values will be done in the space of the monthly differences to avoid problems that may be caused by the different local reference frames, and we will use a neural network for this purpose. The network acts as a time stepping operator (backwards in time) that has two timesteps, n and n-1, at

the input hindcasting timestep n-2. While [3] restricted the training of the network to examples that have three subsequent timesteps with complete data, we will introduce an improved way to train the network that uses all available data. It is similar to the adjoint method used e.g. in data assimilation and was inspired by reading the appendix in [5].

Details about the used "backpropagation" neural network can be found e.g. in [3] or [5]. Here we will give only the transfer function:

$$\mathbf{Y}_{n-2} = b_o + \mathbf{O} \cdot \tanh\left(b_h + \mathbf{H} \cdot \{\mathbf{X}_n, \mathbf{X}_{n-1}\}\right) \quad (1)$$

where $\mathbf{Y}_{n-2}$ is the response of the network to the stimulus $\{\mathbf{X}_n, \mathbf{X}_{n-1}\}$. b_h and b_o are the bias elements of the hidden and the output layer, respectively. $\mathbf{H}$ represents the transfer matrix from the input to the hidden layer and $\mathbf{O}$ from the hidden to the output layer. With $\mathbf{D}_n = \{d_{n,k}\}$ being the vector of TG data at timestep n and $\mathbf{Y}_n = \{y_{n,k}\}$ the output of the neural network corresponding to that timestep then the input $\mathbf{X}_n = \{x_{n,k}\}$ is given by:

$$x_{n,k} = \begin{cases} y_{n,k} & \text{if } d_{n,k} = undef \\ d_{n,k} & \text{otherwise} \end{cases} \quad (2)$$

at which the initial conditions $\mathbf{Y}_N$ and $\mathbf{Y}_{N-1}$ are (partly) unknown. Thus an incorrect network output at timestep n or n-1 influences the hindcast for step n-2 in case it corresponds to a missing data value. The dimensions of the input and the output layer are given by the number of selected TG's, i.e. there are 356 input and 178 output neurons. For the hidden layer we will use 300 neurons. The unknown matrices $\mathbf{H}$, $\mathbf{O}$ and the bias elements b_h and b_h of the neural network as well as missing values in the initial conditions are estimated by minimizing a weighted least square costfunction $\mathbf{K}$

$$\mathbf{K} = \sum_n \sum_k w_{n,k} \left(y_{n,k} - d_{n,k}\right)^2 + c_r \cdot \left[\frac{n_{dat}}{n_h} \sum_i \sum_j (h_{i,j})^2 + \frac{n_{dat}}{n_o} \sum_i \sum_j (o_{i,j})^2 \right] \quad (3)$$

that includes a ridge regression constraint weighted by c_r to minimize/surpress less important entries in the matrices. n_{dat} are the number of data points and n_h, n_o are the number of entries in the corresponding matrices $\mathbf{H}$ and $\mathbf{O}$, respectively. Prior to applying the neural network the data of the individual TG are scaled to have a root mean square (RMS) value of one. This ensures that the entries in $\mathbf{H}$ and $\mathbf{O}$ are of the same order of magnitude, and the weights $w_{n,k}$ of the data misfit part in (3) can be set to one.

To estimate an optimal value for the weight c_r for the ridge regression constraint a subset of the data is excluded from the costfunction (3) for testing the performance of the network while scanning c_r in the range 0 to 1000. This scan is done for eight different sets of retained data (Fig. 2). First we used four disjunct sets of randomly

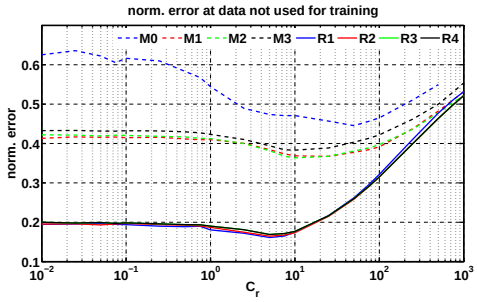

Figure 2. Remaining RMS error at datapoints not used for training depending on the choosen c_r value. See text for details about the eight cases shown. The errors are normalized with the corresponding data RMS.

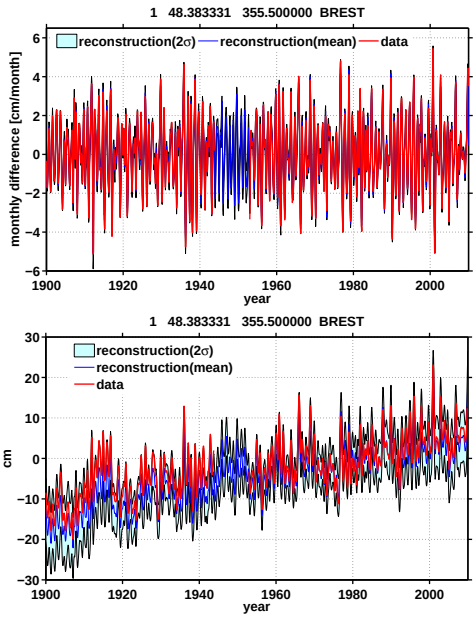

Figure 3. (a) Reconstructed monthly sea level differences at the tide gauge **Brest**, *giving the ensample mean and standard deviation. (b) Cumulative sum of the sea level differences with corresponding error bars.*

choosen data (denoted R1 to R4 in Fig. 2). In the other four cases the data from different periods are retained completely. These periods are M0: [1900-1954]; M1: [1959-1964] and [1996-2001]; M2: [1966-1969], [1976-1979] and [1986-1989]; M3: [1971-1974], [1981-1984] and [1991-1994]. In all of the eight cases about 25% of the data are retained for comparison. After identifying the c_r value with minimum error at the retained data (Fig. 2), the corresponding networks are re-trained using all available data. This finally gives eight realizations of the reconstructed TG time series, where the error of the mean reconstruction stays well between 5 and 10% of the signal RMS.

Timeseries of the reconstructed monthly differences and the corresponding sea level (=cumulative sum) are shown for Brest (Fig. 3) and Manila (Fig. 4) as examples. Differ-

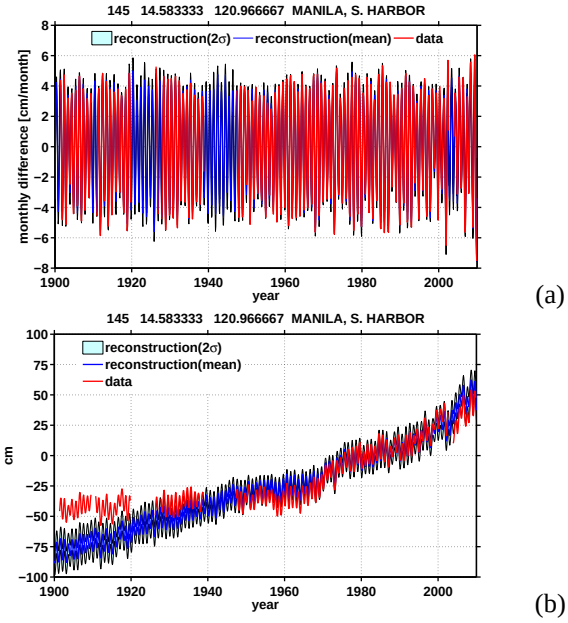

Figure 4. same as Fig. 3 but for the tide gauge **Manila**

ences to the PSMSL data are obvious for the sea level especially for Manila (Fig. 4). A detailed inspection shows that these offsets are caused mainly by the reconstructed values in the gaps. These give a bridging slope different from the one estimated by the PSMSL. Anyhow, we will use only the monthly differences afterwards.

3. GLOBAL SEA LEVEL RECONSTRUCTION

Global sea level anomaly fields are given by satellite altimetry that is available from 1993 onwards. In this study we will use the data taken from the CSIRO sea level web site [6] that don't have inverse barometer correction. These data are processed further as follows: (i) take the monthly differences, (ii) filter the local time series to exclude the annual cycle and (iii) subtract the global mean value. The latter will be treated as the given zero'th principal component (PC) of the following empirical orthogonal function (EOF) decomposition. The resulting first two EOF's are shown in Fig.5 together with the corresponding PC's and the global mean (PC 0). The two leading EOF's / PC's clearly reflect the signals associated with the El Niño–Southern Oscillation (ENSO), while Fig.5c also illustrates the dominance of the local variability compared to the global mean.

The EOF decomposition results in 27 EOF's, whereof 16 are needed to explain 98% of the variance. Thus PC 0 to PC 16 will be reconstructed from the accordingly filtered TG data to give global sea level anomaly fields from 1900 onwards. In [7], [8] or [9] these PC's are estimated by fitting the EOF's to the existing TG values, i.e. they try to reconstruct the TG time series from the altimetry EOF's at the nearest grid point. In view of the poor correlation between the TG measurements and the altimetry that is

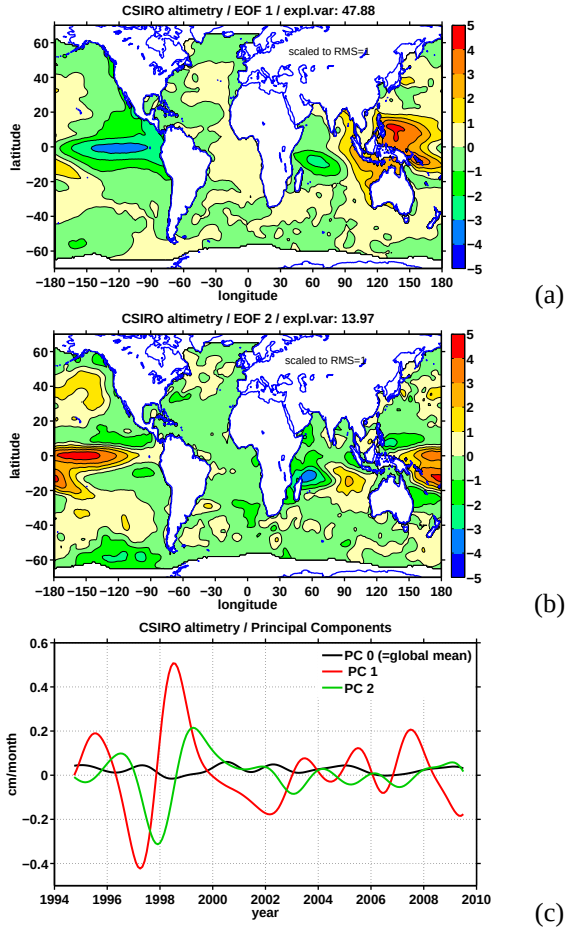

Figure 5. (a) and (b) show the two leading EOF's from the filtered CSIRO altimetry data (monthly differences). The corresponding PC's are given in (c; red and green line) together with the global mean (=PC 0; black line) that was subtracted prior to the decomposition..

found at many positions, especially if the annual cycle is removed, this seems not to be an appropriate way. For this reason each of these principal components, $\mathbf{PC}_k(t)$, will be reconstructed from the TG data matrix $\mathbf{TG}(t)$ by estimating a transfer vector $\mathbf{M}_k$ that provides

$$\mathbf{PC}_k(t) = < \mathbf{M}_k, \mathbf{TG}(t) > \qquad (4)$$

not looking after the EOF's at this point, i.e. the PC values are the weighted sum of the TG values wherein the weights even might be negative. The vector $\mathbf{M}_k$ is estimated from the period where PC data exist via a least square fit and assumed to be valid for the whole period starting from 1900. Eight estimates are made for each PC that differ in whether or not:
i) errors in the tide gauge data are accounted for. In case the standard deviation of the reconstructed ensemble of the corresponding TG is used as noise level (white noise).
ii) a correction of the TG trend is applied to compensate the effect of vertical land movement that is not inherent in altimetry. Following [10] we apply a correction towards the corresponding altimeter trend (nearest grid point) assuming it to be constant in time. A better way would

Table 1. Global mean sea level trend 1900-2009 resulting from different training conditions

	training error	TG-trend correct.	ridge regress.	GMSL trend [mm/year]
1	no	no	no	1.652
2	yes	no	no	1.997
3	no	yes	no	1.196
4	yes	yes	no	1.613
5	no	no	yes	1.832
6	yes	no	yes	1.909
7	no	yes	yes	1.437
8	yes	yes	yes	1.537
	GMSL trend		mean:	1.65 ± 0.26
			from [3]:	1.56 ± 0.25
			from [9]:	1.7 ± 0.2

certainly be the use of measurements taken by the Global Positionig System (GPS) for this, but these are not available for all the tide gauges used.
iii) a ridge regression constraint similar to the one in (3) is applied to the transfer vector **M**. The weights for the individual entries are set to be inverse proportional to the squared correlation between the corresponding TG and the PC under consideration. Thus, the influence of TG's with low absolute correlation will be reduced / suppressed.

The resulting centennial global mean sea level trends are given in Tab.1. The effect of these additional options can be summerized as follows:
i) Accounting for errors in the TG data increases the centennial trend of the global mean sea level (GMSL) but reduces its interannual variability (not shown).
ii) Correcting the TG trends reduces the centennial trend but has nearly no influence on interannual variability.
iii) Introducing the ridge regression constraint leads to an increase of the interannual variability, while the influence on the estimated centennial trend is twofold, it decreases the trend if errors are accounted for but it increases the trend if not.

The mean of the eight reconstructed global mean sea level anomalies is shown in Fig.6 with its error bars. The mean curve fits well to the earlier estimate of [3]. Likewise, the estimate of [9] stays well within the 1-σ errorbar. The mean centennial trend results to 1.65 ± 0.26 mm/year using all eight estimates, which consequently fits well to the trends given by [3] and [9] (see Tab.1). The mean curve in Fig.6 appears as a relatively straight line. The interannual variability is reduced by the averaging, but it is evident in each single estimate and can be deduced from the variability of the decadal trend (Fig.7). The latter varies from $\sim$0.5 mm/year in the early 1950*th* and the late 1980*th* to $\sim$3.0 mm/year at the end of the time series, where it fits to the estimate from the data. These variations are stronger than the ones estimated from the results of [3] but weaker than the ones from [9] although similarities exist with both of these earlier estimates.

In a next step the global sea level anomaly fields are reconstructed by combining the estimated PC's with the altimetry EOF's. From the evolution of these global anomaly fields the local trend can be deduced (Fig.8). For the centennial trend (Fig.8a) we find a very smooth field with positive values ranging from 0 to 2 mm/year nearly all over the ocean. Exceptions are the strong sea level rise in the equatorial Indian Ocean (up to 8 mm/year) and the areas with sea level fall around the Greater Sunda Islands especially west of it (up to -4 mm/year). Most of these local trends are significant at the 1-σ error level. Looking at the fifty-year trends for the periods 1900-1954 and 1955-2009 (Fig.8b and c, respectively) the fields show much more spatial structure, and these structures substantially differ for the periods. Anyhow, the mean values (1.69 mm/year and 1.62 mm/year, respectively) are nearly the same as for the centennial trend (1.65 mm/year). Going to even shorter periods the trends become more variable not only in time (e.g. Fig.7 for the 10 years period) but also in space (not shown). It would be interesting to look if this variability confirms at all to changes in the oceanic forcing fields, but this is beyond the scope of this study.

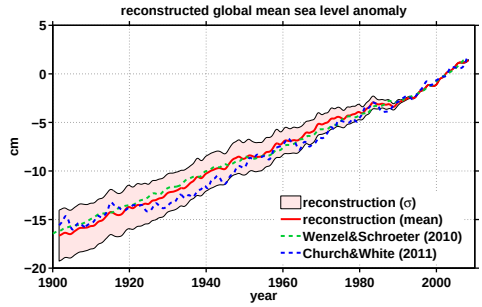

Figure 6. Reconstructed global mean sea level anomaly. Shown are the mean from the training cases given in Tab. 1 together with the standard deviation σ. The results from [3] and [9] are included for comparison.

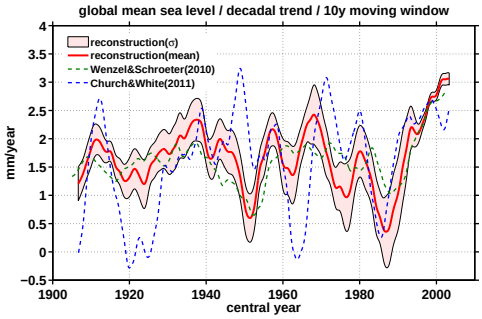

Figure 7. Decadal trend of the reconstructed global mean sea level anomaly estimated from a moving 10 year window. Shown is the mean from the training cases given in Tab. 1 together with the standard deviation σ. The corresponding trends from the results of [3] and [9] are included for comparison.

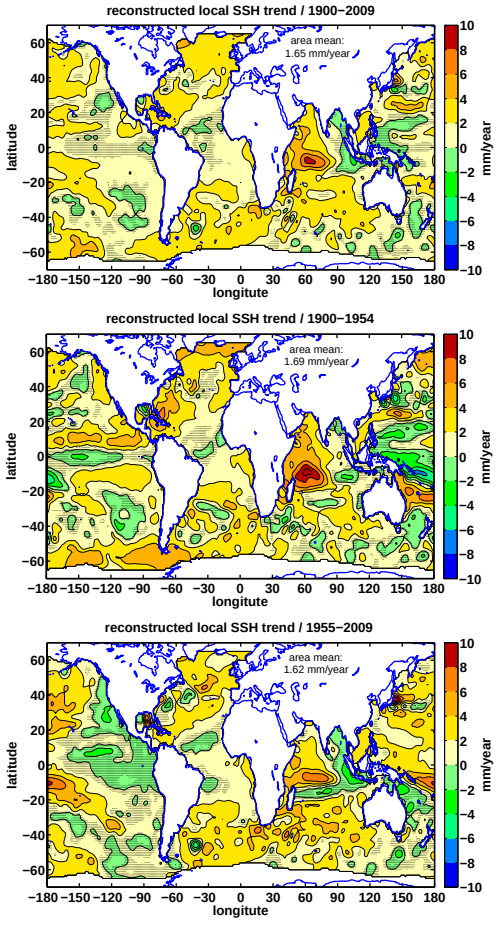

Figure 8. Reconstructed local sea level trend for the periods 1900-2009 (a), 1900-1954 (b) and 1955-2009 (c). Shown are the mean from the training cases given in Tab. 1. In the dotted areas these mean trends are below the corresponding standard deviation σ.

REFERENCES

[1] Church, J., Gregory J., Huybrechts P. et al., 2001, Changes in sea level. In *Climate Change 2001: The Scientific Basis, Contributions of the Working Group I to the Third Assessment Report of the Intergovermental Panel on Climate Change* (Eds. Houghton J.T. et al.), Cambridge University Press, New York, pp. 641–684.

[2] Bindoff N.L., Willebrand J., Artale V., et al., 2007, Observations: Oceanic Climate Change and Sea Level. In *Climate Change 2007: The Physical Science Basis. Contribution of Working Group I to the Fourth Assessment Report of the Intergovernmental Panel on Climate Change* (Eds. Solomon S., et al.), Cambridge University Press, Cambridge, United Kingdom and New York, NY, USA., pp. 385–432.

[3] Wenzel M. & Schröter J., 2010, Reconstruction of regional mean sea level anomalies from tide gauges using neural networks, *J.Geophys.Res.*, 115, C08013, doi:10.1029/2009JC005630.

[4] Woodworth P.L. & Player R., 2003, The permanent service for mean sea level: an update to the 21st century. *J Coastal Res* 19:287–295.
web site: *http://www.psmsl.org*

[5] Hsieh W.W. & Tang B., 1998, Applying Neural Network Models to Prediction and Data Analysis in Meteorology and Oceanography, *Bull.Amer.Meteor.Soc.*, 79, 1855–1870.

[6] CSIRO sea level web site:
http://www.cmar.csiro.au/sealevel/sl_data_cmar.html
file: *jb_ibn_srn_gtn_gin.nc* (downloaded May 03, 2012)

[7] Church J.A., White N.J., Coleman R. et al., 2004, Estimates of the regional distribution of sea level rise over the 1950 to 2000 period, *J.Clim.*, 17, 2609–2625.

[8] Church J.A. & White N.J., 2006, A 20th century acceleration in global sea-level rise, *Geophys.Res.Lett.*, 33, L01602, doi:10.1029/2005GL024826.

[9] Church J.A. & White N.J., 2011, Sea-levcel rise from the late 19th to the early 21th centuary, *Surv.Geophys.*, doi:10.1007/s10712-011-9119-1.

[10] Nerem R.S. & Mitchum G.T., 2002, Estimates of vertical crustal motion derived from differences of TOPEX/POSEIDON and tide gauge sea level measurements, *Geophys.Res.Lett.*, 29(19), 1934, doi:10.1029/2002GL015037.